

1 Revision 1

2

3 Positively-oriented trigons – a unique resorption feature of diamonds from Snap 4 Lake kimberlite dyke, Canada

5

6 Zhuoyuan Li¹, Yana Fedortchouk¹, Alexandrina Fulop², Ingrid L. Chinn³, Njillan Forbes¹

7

⁸ ¹Department of Earth Sciences, Dalhousie University, Halifax, Nova Scotia B3H 4R2,
⁹ Canada

10 ²De Beers Canada; 300-1601 Airport Rd., Calgary, Alberta, T2E 6Z8, Canada

11 ³De Beers Exploration, Private Bag X01, Southdale 2135, South Africa

12

Abstract

14 The role of fluid(s) in the formation of different lithological facies of kimberlites is still
15 poorly understood. The ambiguity of composition of kimberlite melts hampers
16 understanding the composition of volatiles, their depth of exsolution and the effect on
17 magma ascent and fragmentation. Recent estimates of H₂O and CO₂ solubility in
18 kimberlite-like magmas suggest very shallow exsolution of fluid, while many features of
19 kimberlites indicate the presence of significant fluid fraction at depth. Deep magmatic
20 fluid produces negative trigonal etch pits on natural diamonds, the characteristics of
21 which depend on the temperature and composition of the fluid. Positively-oriented
22 trigonal etch pits are very rare on natural diamonds, and are likely a feature of resorption
23 events unique to only some kimberlite magmas. Here we present the first systematic

24 study of positively oriented trigonal etch pits on natural diamonds from Snap Lake
25 kimberlite dyke, Northwest Territories, Canada. The study used 91 micro-diamonds
26 selected from a population of 251 diamonds representative of all six kimberlite litho-
27 facies identified in the Snap Lake dyke. We established that unlike the majority of
28 diamonds from kimberlite pipes in the Northwest Territories, every studied Snap Lake
29 diamond shows positively-oriented trigons. These trigons cover the whole diamond
30 surface starting from the {111} faces and continuing over the resorbed edges. They
31 overprint negatively-oriented trigons and modify them into hexagons. Atomic force
32 microscopy obtained detailed geometry of 154 positive trigons on fourteen diamonds.
33 Three distinct trigon morphologies dependent on the type of the crystal lattice defect
34 were recognized. The point-bottomed shape and positive correlation between the depth
35 and diameter of the individual pits suggest a high CO₂ content in the fluid. Comparison
36 with the existing experimental data on positive trigons implies resorption at low-pressure
37 conditions in the 800-1000°C temperature range by trapped magmatic fluid after the dyke
38 emplacement. The intensity of this late resorption event (and the size of the positive
39 trigons) increases from the dyke contact with the country rock into the interior of the
40 dyke. Such a late resorption event is absent in the majority of kimberlites, which form
41 pipes, and might be a specific feature of hypabyssal kimberlite bodies (dykes). The
42 absence of positive trigons on diamonds from the majority of kimberlites suggests very
43 quick magma cooling below ~800°C after the pipe emplacement, precluding the
44 development of any late resorption features. Our study shows that for kimberlitic magmas,
45 for which mineral chemistry is unable to provide a robust record of magmatic fluid,
46 morphological details of dissolution features on the surface of diamond and other mantle-

47 derived minerals can serve as a fluid proxy. Better constraints of the pressure, temperature
48 and oxygen fugacity of the reversal in the trigon orientation on diamond may help to
49 reconstruct the emplacement path of geologically diverse kimberlite bodies.

50 Keywords: diamond resorption, kimberlitic fluid, Snap Lake kimberlite, trigonal etch pits,
51 atomic force microscope

52

53 **Introduction**

54 Diamonds recovered from kimberlites and other deep-seated mantle magmas show a
55 combination of growth and resorption features on their surfaces. Resorption features are
56 products of diamond dissolution both in the mantle source and in the host magma, while
57 the morphology of these features depends on the conditions in both natural diamond
58 environments. Experiments show that kimberlitic fluid plays a major role in the
59 development of resorption features on diamonds (e.g. Fedortchouk et al. 2007). Thus,
60 better understanding the controls of diamond resorption morphology provides a tool for
61 examining the formation and composition of magmatic fluid during the ascent and
62 emplacement of kimberlite magma, independent of the uncertainty of the primary
63 composition of kimberlite melt (e.g. Moussallam et al. 2016).

64 The common resorption features found on the surfaces of natural diamonds
65 include: etch pits of trigonal, tetragonal, and hexagonal shape, terraces, laminae, hillocks
66 of rounded or sharp shape, and shallow depressions, circular pits, and corrosion
67 sculptures (e.g. Robinson 1979). Trigonal etch pits of negative orientation are a common
68 resorption features (Fig. 1a), which develop via fast propagation of step 2 (Fig. 1a)
69 consisting of carbon atoms doubly bonded to the crystal lattice. Positive trigons are very

70 rarely reported on natural diamonds (Robinson 1979) and develop via fast propagation of
71 step 1 consisting of carbon atoms trebly bonded to the crystal lattice (Fig. 1a) (Yamaoka
72 et al. 1980). Negative trigons are routinely observed in experimental studies conducted at
73 pressures of 1 GPa and higher (Arima and Kozai 2008; Fedortchouk 2007; Khokhryakov
74 and Palyanov 2010) and occur on diamonds from every kimberlite locality and any
75 kimberlite facies. Their maximum size depends on the temperature of the reacting fluid
76 (e.g. Fedortchouk 2015), while shape and abundance is very different in H₂O and CO₂
77 fluids (Khokhryakov and Palyanov 2010, Fedortchouk 2007). Zhang (2016) further
78 examined how the CO₂ content of the reacting fluid affects the relative lengths of the
79 positive (L_{pos}) and negative (L_{neg}) walls of trigonal etch pits (Fig. 1b) where C-O-H fluid
80 with <40 mol% CO₂ produces negative trigons with flat bottomed (f/b) and regular shape;
81 fluid with 40-90 mol% CO₂ produces f/b negative trigons with truncated corners; and
82 fluid with >90 mol% CO₂ produces pointed-bottomed (p/b) trigons and transitional
83 trigon-hexagon form. In addition, dissolution in CO₂-rich fluid produces negative trigons
84 with apparent positive correlation between the diameter and depth of the negative trigons,
85 while in H₂O-rich fluid this relationship is absent (Fedortchouk 2015).

86 Positive trigons have been very rarely reported on natural diamonds (Robinson,
87 1979). Typically, they occur on rare diamond crystals with extremely etched surfaces
88 found in parcels where other diamonds do not show positive trigons. In addition to the
89 positive trigons, these diamonds also show other very rare features, such as transverse
90 hillocks (of the opposite orientation compared to the common hillocks and imbricate
91 wedge markings (Fig. 1c,d). Positive trigons are the most common feature observed in
92 experiments conducted at 0.1 MPa but have been also produced at high pressures (high-P)

93 (e.g. Yamaoka et al., 1980, Harris and Vance, 1974). The causes of the reversal in the
94 orientation of trigonal etch pits on diamonds are still not well understood. Experimental
95 studies observed the change from negative to positive trigons at high oxygen fugacity
96 (fO_2) at 0.1 MPa (Evans and Sauter 1961) and at 1.5 GPa (Yamaoka et al. 1980) and
97 temperatures of 900°C and 1130°C respectively. These authors proposed that T and fO_2
98 control the orientation of the trigons via stabilization of doubly bonded atoms of step 2
99 (Fig. 1a) with oxygen complexes (Evans and Sauter 1961; Yamaoka et al. 1980).
100 Similarly, T and fO_2 control a reversal in the orientation of tetragonal etch pits on {100}
101 diamond faces (Fedortchouk and Canil 2009). However, experiments at 5-7 GPa and
102 1400 – 1750°C (Khokhryakov and Palyanov 2010) produced positive trigons in dry
103 carbonate melt and reversed to negative trigons after addition of 8 wt% of H₂O at the
104 same fO_2 , which allowed the authors to propose that the CO₂:H₂O ratio is the main
105 control for the trigon orientation. On the contrary, Harris and Vance (1974) recorded at
106 0.1 GPa and 1050°C negative trigons in carbonate-rich composition and positive in more
107 H₂O rich compositions. Thus, the existing experimental data does not give an explicit
108 answer on the causes of change in trigon orientation. A theoretical model by Angus and
109 Dyble (1975) proposes that formation of positive trigons requires preferential removal of
110 triply bonded carbon atoms, which requires more energy than removal of the doubly
111 bonded atoms that accompanies negative trigon formation. Better understanding of the
112 controls of the trigonal etch pit orientation on diamonds may help to constrain
113 crystallization conditions of kimberlite magma.

114 Snap Lake kimberlite dyke (Northwest Territories, Canada) is a unique example
115 of a kimberlite body, where all diamonds show positive trigons. What makes Snap Lake

116 so unique? Are the positive trigons on Snap Lake diamonds a product of deep (high-P)
117 resorption due to the different kimberlite emplacement conditions than the majority of
118 kimberlites, or do they represent a different resorption event happening at shallow near-
119 surface conditions in a hypabyssal kimberlite body as opposed to the typical kimberlite
120 that bursts through the earth's surface to form a pipe? Can we deduce the crystallization
121 conditions of the Snap Lake kimberlite(s) using the morphology of positive trigons? We
122 address these questions via a detailed study of the positive trigons on diamonds from
123 different litho-facies of the Snap Lake kimberlite dyke. Employment of an Atomic Force
124 Microscope (AFM) for study of diamond surface features allowed us not only to detect
125 the presence of small-sized trigons, but also to examine how the shape and dimensions of
126 the trigons vary throughout the kimberlite body. Here we report the first systematic study
127 of the morphology and characteristics of positive trigons on natural diamonds recovered
128 from known sections of a single kimberlite body. The study aims to understand what
129 factors control the presence, morphology, and dimensions of the positive trigons, and to
130 examine their distribution within the Snap Lake dyke in order to better understand the
131 role of volatiles in kimberlite emplacement.

132 **Background geology and diamond samples**

133 The Snap Lake Mine is located in the southeastern part of the Slave Craton about
134 220 km northeast of Yellowknife, Canada (Fig. 2a) (Fulop et al. 2017). The age of the
135 kimberlite, 535–523 Ma, was determined by Rb-Sr dating of phlogopite (Agashev et al.
136 2001; Heaman et al. 2003, 2004). The country rocks comprise granodiorites, tonalities
137 and granites of the Defeat Pluton Suite (2610 – 2590 Ma) and metavolcanic rocks of the
138 Yellowknife Supergroup (Stubley 2000). There is no evidence of a thermal aureole in the

139 country rocks adjacent to the intrusion (Gernon et al. 2012). The orebody of the Snap
140 Lake kimberlite is a segmented hypabyssal dyke dipping 12-15° towards the northeast
141 flanked by a series of subparallel sheets (Gernon et al. 2012; Kopylova et al. 2010). The
142 thickness of the dyke ranges from 0.1 to 15 m, but typically ~ 3-5 m (Gernon et al. 2012).

143 The Snap Lake dyke is filled with a coherent hypabyssal kimberlite HK
144 (following the terminology of Scott Smith 2013) with minor kimberlite breccia facies
145 dominated by granite or amphibolite xenoliths (Kopylova et al. 2010; Mogg et al. 2003).
146 Two models have been proposed to explain the compositional variation and the
147 emplacement of the Snap Lake dyke. A two magma batches model suggests that the two
148 different litho-facies (the main olivine-rich and phlogopite-poor facies, and the
149 subordinate phlogopite-abundant facies) evolved from two magma batches which co-
150 mingled and intruded almost simultaneously (Gernon et al. 2012; Ogilvie-Harris et al.
151 2008; Field et al. 2009). A single magma batch model suggests formation of one
152 hypabyssal kimberlite with different degrees and forms of deuterian alteration and crustal
153 contamination responsible for the generation of six sublitho-facies from HK1 to HK6,
154 which is supported by petrographic, geochemical, and mineral chemistry data (Mogg et al.
155 2003, Kopylova et al. 2010, Fulop et al. 2017). The middle of the dyke is composed of the
156 freshest phlogopite-poor HK1 and HK2 facies, with more altered HK5 surrounding
157 granitoid xenoliths. The progressively more altered phlogopite-rich HK3, HK4 and HK6
158 facies developed at the contact with the country-rock granitoids (Fig. 2b).

159 Our study used 251 micro-diamonds provided by De Beers Canada Inc with the
160 maximum diamond size 1.7 mm. We selected 91 diamonds that are ≥300 µm in size and
161 can be handled under an optical microscope (diamonds <300 µm are mostly fragments

162 and provide no information about resorption of crystal faces) and that are not fragments
163 or show at least 50% of the crystal faces, so that crystal morphology can be studied. Our
164 study focused on octahedral or tetrahexahedral (THH) diamonds, since cubic diamonds
165 are lacking experimental data on their resorption. The selected 91 diamonds comprise 78
166 octahedral and 13 THH diamonds, which represent all litho-facies at Snap Lake: HK1 (25
167 diamonds), HK2 (25 diamonds), HK3 (4 diamonds), HK4 (14 diamonds), and HK5-HK6
168 (23 diamonds). AFM was conducted on 16 diamonds representing all litho-facies and
169 Fourier transform infrared spectroscopy (FTIR) measurements were obtained for 82
170 diamonds (including few fragments). The diamonds were recovered at Saskatchewan
171 Research Council (SRC) by caustic fusion at 500°C in Na(OH)₂. Use of test synthetic
172 diamonds with every batch confirms no etching during the recovery process.

173

Analytical methods

174 **Optical and Scanning Electron Microscopy (SEM)**

175 The diamonds were initially studied using a stereomicroscope to examine the general
176 morphology, color, color intensity, and the presence of inclusions. Further examination of
177 growth/resorption features on diamond surfaces and grouping into morphological types used a
178 stereomicroscope and reflected light on a petrographic microscope with partially closed aperture
179 stop for increased contrast. We classified diamonds with more than 10% of {111} faces
180 preserved as an octahedron, and with less than 10% of {111} faces preserved – as a
181 tetrahedron (THH). The morphologies of twinned diamonds and aggregates were classified
182 based on the dominant shape of the constituent crystals. The octahedral diamonds were further
183 divided into several morphological groups based on: (1) trigonal vs. ditrigonal shape of {111}
184 faces, and (2) the type of resorption features on the {111} face including step faces, etch pits
185 (negative and positive trigons, trigon-hexagons, hexagons), and laminae (shield-shaped, serrate-
186 or irregular-shaped). SEM examination of 29 representative diamond crystals further refined the
187 morphological grouping. Positive trigons larger than 1 μm were recorded with an optical
188 microscope. The presence of positive trigonal etch pits smaller than 1 μm on the studied
189 diamonds was confirmed with SEM. Diamonds selected for SEM were cleaned with a boiled
190 $\text{HNO}_3\text{-H}_2\text{SO}_4$ mixture (3:5 volume proportion) at $\sim 200^\circ\text{C}$ for at least 30 min followed by
191 ultrasonic cleaning in distilled water for 15 min and were then coated with gold. We used a Field
192 Emission Scanning Electron Microscope (FE-SEM) Hitachi S-4700 FEG at the Institute of
193 Research in Materials, Dalhousie University, with accelerating voltage of 10-15 kV and beam
194 current of 15 μA .

195 **Atomic Force Microscopy (AFM)**

196 The AFM study of 16 diamonds (positive trigons were studied on 14 diamonds) was
197 conducted using a Veeco Multimode 8 atomic force microscope at the Department of Earth
198 Sciences, Dalhousie University. The diamonds were cleaned with aqua regia ($\text{HNO}_3\text{-HCl}$ in 1:3
199 volume proportion) to remove the gold coating and other possible metal impurities, and then
200 with a $\text{HNO}_3\text{-H}_2\text{SO}_4$ mixture (3:5 volume proportion) to remove the carbon from the SEM tapes
201 and other dirt. During both treatments, the diamond crystals were boiled at $\sim 200^\circ\text{C}$ for at least 30
202 minutes. Finally, the crystals were cleaned in distilled water in an ultrasonic bath for 15 minutes.
203 Prior to the AFM measurements, all selected diamonds were photographed at 100 \times and 200 \times
204 (500 \times for minute features such as positive trigons) magnification using a petrographic
205 microscope. Each diamond was mounted on a steel disk with an adhesive pad, in an attempt to
206 orient the examined {111} face horizontally. In the case of uneven or fragmented crystals glue
207 from the adhesive tape was placed under the crystal to minimize the tilt. All AFM images were
208 collected using a J scanner (Bruker, maximum coverage 125 $\mu\text{m} \times 125 \mu\text{m} \times 5 \mu\text{m}$ in x, y and z
209 dimensions), operated in contact ScanAsyst mode using ScanAsyst Air Probes (Bruker, silicon
210 tip on nitride lever, spring constants 0.4 to 0.8 N m^{-1} , resonant frequency 50-90 kHz, nominal tip
211 radius of curvature 2 nm). The scanned areas ranged from 5 \times 5 μm to 80 \times 80 μm . The scanning
212 frequency was dependent on the size of the scanned areas: we used 0.2 – 0.4 Hz for areas greater
213 than 30 \times 30 μm and 0.5 – 0.8 Hz for smaller areas to optimize the match between the trace and
214 retrace lines. All the scans were conducted with 512 sample lines.

215 The images were analyzed using NanoScope software (v8.10) after a “plane fit” function
216 to remove the tilt in both x and y directions. The parameters of individual etch pits (diameter,
217 depth, shape, wall angles) were examined on cross-section profiles using the section analyses
218 tool. A profile was drawn from the middle of a trigon side to the opposite vertex. For each

219 diamond we routinely measured 8–20 positive trigons. We measured the diameter of the pits as a
220 distance between the middle of one side and the opposite vertex, the depth of the pits as the
221 distance between the {111} face and the bottom of the pit, and the wall angles ($\alpha_{\{111\}}$) as the
222 angle between the plane of the wall micro-face and (111) plane. Each parameter comprises an
223 average of the three measurements for the profile drawn from each of the three pit vertexes. The
224 pits were classified based on the bottom and wall morphology (Fig. 3) (see also Zhang et al.
225 2015). The three sources of uncertainties in AFM measurements include: (1) the AFM
226 uncertainty (1.4% in x, y and z directions); (2) a possible tilt of the {111} diamond face; (3) the
227 subjective selection of the measurement (the placement of the profile line and the markers used
228 for the measurements). We estimate the total uncertainty <2.5% for diameter measurement, <6%
229 for depth measurement, and <4° angle measurement (Table 1) (see also Zhang et al. 2015; Li
230 2017).

231 Fourier transform infrared spectroscopy (FTIR)

232 Nitrogen content and aggregation state were obtained with Fourier transform infrared
233 spectroscopy (FTIR) for the 14 diamond crystals with positive trigons studied by AFM (Table 2).
234 Diamond crystals were mounted on the edge of a glass slide with the (111) faces perpendicular to
235 the FTIR beam. We used Thermo-Nicolet Nexus 470 FTIR spectrometer fitted with a
236 Continuum infrared microscope equipped with a KBr beam splitter at the Department of Earth
237 and Atmospheric Sciences at the University of Alberta. Absorption spectra were measured in
238 transmission mode in the range of 4000–650 cm⁻¹ with a resolution of 8 cm⁻¹, and were collected
239 for 200 s through a 100 × 100 μm² aperture. Sample spectra were first baselined using the Basic
240 Macro of the OMNIC 32 software suite. A normalized Type II diamond spectrum used as a
241 standard for background correction was subtracted from the spectra to convert absorbance to

242 absorption coefficient. After the conversion, sample spectra were de-convoluted into the A, B
243 and D components using least square techniques (for more details see Stachel et al. 2006, Boyd
244 et al. 1994, 1995). The detection limit for nitrogen is about 10 ppm and the analytical precision is
245 10-20 % of the concentration (Stachel et al., 2006).

246 **Diamond etching experiments**

247 The temperature limit for the development of any resorption features on diamond at 0.1 MPa was
248 tested in experiments conducted at 700°C and 800°C at oxygen fugacity (fO_2) corresponding to
249 that of the air ($\log fO_2 = -0.68$) using a box furnace and at fO_2 corresponding to that of CO₂ gas
250 ($\log fO_2 = -2.85$ at 700°C and -2.79 at 800°C) using a vertical-tube gas-mixing furnace in the
251 Department of Earth Sciences at Dalhousie University. In both cases, natural octahedral
252 diamonds (weight ~0.5 – 1 mg) with minimal natural resorption were imaged with AFM to
253 record any pre-existing features, placed inside Al₂O₃ crucible, and covered with a synthetic
254 mixture of 45 mol% Na₂CO₃ and 55 mol% NaCl corresponding to the eutectic composition with
255 melting temperature 632°C. The run duration was 2.5 hours in the air runs and 3 hours in CO₂
256 runs. After the experiments the diamonds were recovered, cleaned following the described above
257 procedure, and imaged with optical microscope and AFM to detect any new features on the
258 diamond's surfaces.

259 **Results**

260 **General morphologies and negative trigons of Snap Lake diamonds**

261 We divided the octahedral and THH diamonds from Snap Lake into twelve
262 morphological groups based on the shape of {111} faces (trigonal vs. ditrigonal) and the type of
263 the surface resorption features. The details of morphological groupings and full description of the
264 negative trigonal etch pits will be reported elsewhere. Here we focus on the features of the

positive trigons. The 14 diamonds for which positive trigons were studied with AFM are all colourless octahedra, which represent eight morphological groups illustrating both mantle-derived and kimberlite-induced resorption (Fig. 4). The number of negative and positive trigons analyzed on each diamond is reported in Table 2. AFM study of the negative trigons revealed that they all have regular flat-bottomed (f/b) shape, diameter $< 45 \mu\text{m}$, and depth $< 1 \mu\text{m}$. The unique feature of all negative trigons on Snap Lake diamonds is their truncated corners to a degree that makes them transitional into hexagons (Fig. 5e,f). Many negative trigons contain small positive trigons inside (Fig. 5b,c,f) or along their perimeter (Fig. 5a,d).

Positive trigons on Snap Lake diamonds

All 91 studied diamonds from Snap Lake kimberlite have positive trigons, which cover both octahedral and THH faces. While negative trigons are limited to $\{111\}$ faces, positive trigons occur also on the rounded THH edges of resorbed diamonds (Fig. 6a,b). Positive trigons are distributed uniformly (Fig. 6a) or show a patchy uneven distribution of larger and smaller trigons in different areas of $\{111\}$ faces (Fig. 6c). They also enhance the development of wormy depressions (ruts) (Fig. 6h). The majority of the positive trigons have a diameter $< 3 \mu\text{m}$, which correlates with their depth (Fig. 7). Diamonds from HK1 and HK2 facies have larger trigons and only two of the fourteen diamonds (SNP8-9 and SNP9-1) have positive trigons with diameters larger than $4 \mu\text{m}$ (up to $13 \mu\text{m}$). Less resorbed diamonds have positive trigons with diameter $\leq 0.5 \mu\text{m}$ and depth $< 20 \text{ nm}$, which could only be detected using SEM or AFM. The diameter of the positive trigons roughly correlates with the kimberlite lithology and decreases from fresh (HK1 and HK3) and slightly altered facies (HK2 and HK4) towards highly altered facies (HK5 and HK6) (Fig. 8). Diamonds from HK2 show three larger diameter trigons in Fig. 8, which

287 might be a result of an overprint of pre-existing pits. We found no correlation between the size of
288 the positive trigons and the general diamond morphology.

289 The detailed AFM study of 154 positive trigons on 14 Snap Lake diamonds (reported in
290 Supplementary Table 1) allowed us to divide them into four groups (Fig. 9):

291 1) point-bottomed (p/b) trigons with an irregular outline and walls consisting of multiple
292 micro-steps (Fig. 9b)

293 2) trigons similar to above but the bottoms are curved (c/b) and not pointy; the walls have
294 V or U shape; trigons with simple corners have more rounded bottoms (Fig. 9c), while trigons
295 with multiple corners have flatter bottoms (Fig. 9d)

296 3) asymmetric trigons with straight outlines and regular steps along one of the walls,
297 shallower pits are f/b (Fig. 9e) and deeper pits are p/b (Fig. 9f)

298 4) trigons with truncated corners and transitional trigon-hexagons with straight walls and
299 well-defined f/b shape (Fig. 9g)

300 The shape (f/b vs. p/b) of the small embryonic trigons with diameter <1 μm and depth <
301 100 nm (e.g. Fig. 9a) cannot be reliably distinguished with the scanner used. P/b is the most
302 prevalent shape of the positive trigons on Snap Lake diamonds; only transitional trigon-hexagon
303 pits show regular f/b shape and most likely represent an overprint of positive trigons on small
304 pre-existing negative trigons.

305 There are two distinct trends on diameter vs. depth plots (Fig. 7) where p/b trigons form a
306 steeper slope and c/b trigons form a shallower slope. P/b trigons are the most common and occur
307 on the majority of the studied diamonds. They form the only trigon type on the three diamonds
308 from HK1 and HK2 (SNP2-1, SNP8-9, SNP3-6). Asymmetric trigons are limited to only two
309 diamonds from HK1 and HK2 (SNPO13-2, SNPO9-1), that also show highly intensive etching

310 of {111} face. These trigons evolve from f/b to p/b as their depth increases. Curved c/b trigons
311 appear alone (SNP3-8) or in combination with p/b trigons (SNP6-1, SNP9-1, SNPO12-13,
312 SNP12-8). Trigons with flatter bottoms mostly occur on diamonds from phlogopite-rich altered
313 facies HK4 and HK6. Trigon-hexagon f/b pits were only observed on two diamonds from the
314 altered facies at the contact with granitoids of HK5 (phlogopite-poor) and HK6 (phlogopite-rich)
315 kimberlites (SNP5-3, SNPO12-2). The wall type of the studied trigons shows an evolution from
316 U to V to Y as the depth of the trigons increases on the same diamond (Supplementary table 1).

317 **Experimental result**

318 In this study we only focused on the presence of absence of any changes to diamond surface after
319 heating in sodium carbonate-chloride melt at 700°C and 800°C and $\log fO_2 = -0.68$ (air), -2.79
320 and -2.85 (CO₂). Fig. 10 shows that etching at 800°C developed positive trigons on diamond
321 surface easily seen on the micro-photographs taken under an optical microscope. After 700°C
322 runs, no changes were visible under an optical microscope, but AFM showed development of
323 positive trigons only in the run with air. AFM imaging detected no changes on diamond surface
324 after the run at 700°C in CO₂.

325 **Discussion**

326 **Where do positive trigons form?**

327 In experiments positive trigons form over a wide pressure range: at 0.1 MPa (Evans and Sauter
328 1961), 0.1 GPa (Harris and Vance, 1974), 1.5 GPa (Yamaoka et al. 1980), 5-7 GPa
329 (Khokhryakov and Palyanov 2010). The distribution patterns of positive trigons on natural
330 diamonds from Snap Lake kimberlite support the conclusion of Robinson (1979) these positive
331 trigons are a feature of the latest resorption event, which can overprint previous resorption.
332 Indeed, positive trigons cover the whole diamond surface including the rounded resorbed faces

333 (Fig. 6) and bottoms of the larger negative trigons. Furthermore, the AFM images obtained in our
334 study demonstrate that positive trigons on Snap Lake diamonds overprint all the pre-existing
335 negative trigons. They are present on the bottoms, along the sides or in the center of the negative
336 trigons, and add truncated corners to all the negative trigons resulting in their transition to trigon-
337 hexagon and hexagon shapes (Fig. 5a-f). Our results demonstrate that the presence of positive
338 trigons on Snap Lake diamonds records conditions of a particular late resorption event.

339 Reversal in the trigon orientation manifested in the formation of trigon-hexagonal and
340 hexagonal pits has been observed during diamond dissolution in CO₂-rich fluid (Fedortchouk et
341 al. 2007, Khokhryakov and Palyanov, 2010). Zhang (2016) found that truncation of the corners
342 of negative trigons starts when CO₂ constitutes more than 50 mol% of the fluid and hexagons
343 form at CO₂ content >95 mol%, where the ratio L_{pos}/(L_{pos}+L_{neg}) can be used to quantify the
344 degree of trigon to hexagon transformation (Zhang, 2016). If the development of positive walls
345 inside the negative trigons on Snap Lake diamonds was controlled by the CO₂ content of the
346 magmatic fluid, as in the Zhang (2016) experiments, both negative and positive walls of
347 truncated trigons and trigon-hexagon pits would have developed simultaneously during a single
348 resorption event so that the L_{pos}/(L_{pos}+L_{neg}) ratio would be independent of the diameter of the pit.
349 In such a case, a correlation with the kimberlite lithology would be expected. If the formation of
350 the positive walls overprinted the original shape of a negative trigon, then the L_{pos}/(L_{pos}+L_{neg})
351 ratio would show a negative correlation with the trigon diameter. Fig. 11a shows the correlation
352 for the studied Snap Lake diamonds, where the smaller the diameter of the negative trigons the
353 larger is their L_{pos}/(L_{pos}+L_{neg}) ratio. Fig. 11a also shows a different trend for HK1 and HK2
354 diamonds with a larger L_{pos}/(L_{pos}+L_{neg}) ratio for the same diameter compared to the diamonds
355 from the other lithologies. Diamonds from HK1 and HK2 also have a larger absolute value of

356 L_{pos} (Fig. 11b) and larger diameter of the positive trigons (Fig. 8) indicating the higher intensity
357 of the resorption event forming positive trigons in the HK1 and HK2 kimberlite facies. The
358 micro-features on the positive walls of truncated negative trigons on Snap Lake diamonds are
359 different from those produced in CO₂-rich dissolution experiments by Zhang (2016) (Fig. 5g-i).
360 In these experiments, the truncation by positive wall development was accompanied by a
361 curvature of the negative trigon walls (Fig. 5g-i). All this evidence confirms that trigon-
362 hexagonal and hexagonal pits on Snap Lake diamonds are not a product of resorption in more
363 CO₂-rich fluid but a combination of two resorption events – an early (high-P) event, that
364 produced negative trigons typical for the majority of kimberlitic diamonds, and the later (low-P)
365 event, that produced positive trigons and truncated negative trigons, a specific feature of the
366 Snap Lake diamonds.

367

368 **Application to Snap Lake kimberlite system**

369 This late resorption event in the Snap Lake kimberlite most likely occurred after dyke
370 emplacement, while the kimberlite was still at magmatic temperature. Experimental studies of
371 diamond etching help to constrain the temperature of this late resorption event responsible for the
372 development of the positive trigons on Snap Lake diamonds. Yamaoka et al. (1980) estimated
373 1130°C as a reversal temperature from negative to positive orientation of trigonal etch pits at 1.5
374 GPa. Slightly lower reversal temperature between 900 and 1000°C obtained by Evans and Sauter
375 (1961) at more oxidized conditions cannot be explained by the difference in f_{O_2} , which according
376 to Yamaoka et al. (1980) should increase the reversal temperature at higher f_{O_2} . Most likely the
377 reason for this discrepancy is in erroneous f_{O_2} estimates in Yamaoka et al. (1980). Their study
378 used a double capsule technique with an oxide buffer in the outer capsule and diamond crystals

379 in the small capsule inside. Such an approach requires reaching equilibrium in the system, which
380 cannot be achieved until the diamonds are completely oxidized. As long as the diamond
381 oxidation reaction proceeds the f_{O_2} would be somewhere between the value imposed by the oxide
382 buffer and the value of the CCO buffer. Thus, we suggest 900 - 1000°C as the maximum
383 temperature for the development of positive trigons on Snap Lake diamonds, which is slightly
384 below the ~1100°C crystallization temperature of kimberlite magma (Fedortchouk and Canil
385 2004).

386 The minimum T for this resorption event is the T limit for diamond resorption. According
387 to the experiments of Yamaoka et al. (1980) this is 800°C. A number of studies (e.g. Evans and
388 Sauter 1961, Phaal 1965) observed diamond etching at temperatures as low as 650°C but only in
389 pure oxygen, and above 950°C in CO₂ flow. Our experiments conducted at yet more oxidized
390 conditions than that of natural kimberlites show that at 700°C resorption occurs in the air but
391 does not proceed in pure CO₂ gas corresponding to $\log f_{O_2} = -2.85$ (Fig. 10). We propose the
392 temperature of the late resorption event forming positive trigons on diamonds from Snap Lake
393 dyke between 800 – 1000°C.

394 Kimberlite magma typically arrives at the earth's surface with substantial amounts of
395 magmatic fluid formed via CO₂ degassing accompanying assimilation of silicate xenoliths by
396 carbonate-rich magma (e.g. Russell et al. 2012; Stone and Luth 2016) as well as from
397 decompressional degassing of H₂O and CO₂ in the last few km of the ascent (Moussalam et al.
398 2016). Extensive serpentinization and other alteration reactions observed in kimberlites can be a
399 product of reaction with the magmatic fluid (e.g. Mitchell 2013) or can result from a substantial
400 contribution from meteoric fluid (e.g. Stripp et al. 2006). The high content of phlogopite in Snap
401 Lake kimberlite, especially closer to the contact with the country-rock granitoids (HK3,4,6 facies)

402 was interpreted as a product of alteration by deuteritic fluid (Fulop et al. 2017). The dimensions of
403 the positive trigons on diamonds can help to examine the nature of the fluid during the late
404 resorption event at Snap Lake. The diameter of the trigonal etch pits on diamonds depends on T
405 and the duration of the diamond reaction with fluids (Fedortchouk 2015). The largest diameters
406 of the positive trigons on diamonds from our study are limited to the two freshest facies (HK1
407 and HK2, Fig. 8) present in the interior parts of the intrusion far from the contact with the
408 country rock. Diamonds from the facies closer to the contact with the granitoid (HK3,4,6) or
409 surrounding large granitoid xenoliths (HK5) (Fig. 2b) show very small sizes of the positive
410 trigons. This implies longer interaction with fluid possibly at higher T in the interior parts of the
411 intrusion. In combination with the estimated high T of the late resorption event, this would
412 strongly support magmatic fluid as the resorption agent. We propose that at depth, during the
413 ascent of the Snap Lake kimberlite magma to the surface, magmatic fluid gave rise to resorption
414 features typical for all kimberlite-hosted diamonds (such as negative trigons). After the
415 emplacement, the fluid was trapped in this hypabyssal intrusion close to the surface, and resulted
416 in the later resorption event manifested in the development of the positive trigons on Snap Lake
417 diamonds, which is not present on diamonds from both volcaniclastic and coherent lithologies in
418 kimberlite pipes in Ekati Mine, Canada, and Orapa kimberlite cluster, Botswana (Fedortchouk et
419 al 2010; Fedortchouk et al. 2017).

420 However, Snap Lake may not be that unique. Many diamonds from this study have so
421 small trigons, which were only detected with SEM, and would have been overlooked during a
422 routine examination under an optical microscope even with 50x objective. Indeed, AFM
423 scanning of octahedra micro-diamonds from unknown Yakutian sources used for diamond
424 dissolution experiments have shown presence of positive trigons on some diamonds

425 (Fedortchouk, unpublished data). Furthermore, there is only very limited data on diamonds from
426 kimberlite sheets. Some of them are not diamondiferous, others are too thin to be mined.
427 Diamonds from kimberlite pipe are lacking such widespread development of positive trigons,
428 and only show them on rare individual diamonds in association with other very rare features (Fig.
429 1 c,d). It is possible that a late resorption event forming positively-oriented trigons is a feature of
430 kimberlite sheets. The fluid responsible for the late resorption is clearly not related to
431 serpentinization that occurs at low temperatures around 130–400°C (Afanashev et al. 2014) and
432 creates strongly reducing conditions (McCollom and Seewald 2013).

433 The shape of negative trigons on diamond can be used to deduce the H₂O:CO₂ ratio in the
434 reacting fluid (Fedortchouk 2015). Twelve out of fourteen diamonds studied by AFM show two
435 types of positive trigons: 1) p/b trigons with straight walls (which evolve from small flat almost
436 f/b pits, Fig. 9a,b), and 2) curved-bottom trigons (Fig. 9c,d). Both types of trigons form distinct
437 positive trends of diameter vs. depth (Fig. 7), the slope of which is steeper for p/b trigons and
438 shallower for curved/bottomed trigons. Study of the negative trigons from diamond dissolution
439 experiments (Fedortchouk 2015) suggests that such trigon morphologies and the positive
440 correlation between the diameter and the depth are indicative of CO₂-rich fluid. However,
441 applicability of this correlation to positively oriented trigons has yet to be confirmed
442 experimentally. Negative trigons on Snap Lake diamonds show very regular f/b shape of the
443 diamonds that suggests predominantly aqueous fluid in the earlier high-P resorption event during
444 the magma ascent (Fedortchouk et al. 2007; Fedortchouk 2015). The shape of the positive trigons
445 would agree with the fluid evolution towards more CO₂-rich composition after the emplacement
446 during crystallization of the dyke, given that CO₂ effect on the shape of positive and negative
447 trigons is similar. Assimilation reactions between the carbonate component of the melt and

448 silicates from the granitoids may have provided an additional CO₂ input. Alternatively, the
449 difference in the shape of negative and positive trigons can be related to the different dissolution
450 conditions during the earlier (high-P) and late (near-surface) resorption events. Luttge (2006)
451 proposed that at conditions close to equilibrium (small ΔG), crystal dissolution proceeds via
452 formation of flat-bottomed “pancake” pits growing around kinks associated with point defects.
453 When the conditions are far from equilibrium (at higher ΔG), dissolution opens the hollow cores
454 at screw dislocations forming deeper p/b etch pits. Pressure has a large control on the stability of
455 the diamond lattice. A decrease in pressure shifts the system very far from an equilibrium
456 (towards larger ΔG). The presence of large diameter but shallow negative trigons and the
457 absence of such shallow positive trigons on Snap Lake diamonds might be due to much higher
458 ΔG at low P.

459 Development of both f/b and p/b asymmetric trigons is limited to only three diamond
460 crystals, of which two have no other trigon types (Fig. 7, SNPO13-2, SNPO9-1). This is likely
461 not due to the external conditions of the resorption but the internal properties of these diamond
462 crystals and their defects. Finally, truncated and trigon-hexagonal pits were only observed on
463 diamonds from kimberlite facies very close to the contact with large xenoliths (HK5) or country-
464 rock (diamond SNPO12-2 from HK6, Fig. 7). Incomplete transformation of very small (<2 μm in
465 diameter) negative trigons into positive trigons, suggests a very short duration of resorption and
466 confirms the increase in the resorption intensity towards the center of the dyke.

467

468 **Mechanism of diamond resorption and development of positive trigons**

469 Review of the existing experimental data shows uncertainty in the conditions required for
470 formation of negative vs. positive trigons on diamonds during dissolution. Yamaoka et al. (1980)

471 following Evans and Phaal (1962) and Phaal (1965) propose that T and fO_2 affect the activity of
472 oxygen in stabilizing certain directions of the diamond lattice via C – O – C bridges (Fig. 1a).
473 However, evolution from negative trigons to hexagons and positive trigons was observed in
474 experiments at the same T, P, and fO_2 , but conducted in H₂O-rich and CO₂-rich systems
475 (Fedortchouk et al. 2007; Khokhryakov and Palyanov 2010; Zhang 2016) emphasizing the role
476 of water in the orientation of etch pits on diamond. Angust and Dyble (1975) developed a
477 theoretical model based on an ideal configuration of diamond crystal lattice (Fig. 12), which
478 proposed that development of negatively-oriented trigons is expected for the diamond lattice
479 because this mechanism involves preferential removal of carbon atoms bonded to fewer of the
480 surrounding atoms. On the contrary, the development of positively-oriented trigons requires
481 conditions with no preferential removal of triply-bonded and doubly-bonded carbon atoms. This
482 could be achieved when the diamond crystal lattice becomes very unstable, such as at very low P
483 or very high fO_2 . Since diamond is a high-pressure carbon phase, emplacement of kimberlite
484 magma at shallow levels could create conditions where the diamond lattice becomes extremely
485 unstable, the activation energy needed to remove triply-bonded and doubly-bonded atoms
486 become similar, and positive trigons start to form. This agrees well with the observed occurrence
487 of positive trigons on diamonds from the shallow Snap Lake kimberlite sheet but their absence
488 on diamonds from Ekati kimberlite pipes both located in Slave craton of Canada (e.g.
489 Fedortchouk et al. 2010). Indeed, most of the experiments on diamond dissolution or oxidation
490 report positive trigons at 0.1 MPa and negative trigons at elevated P. While low pressure is not
491 the only possible way to destabilize diamond and produce positive trigons, it appears to be the
492 most likely cause in natural kimberlitic systems.

493 Positive trigons developed in high-P experiments accompany features of extreme
494 diamond etching. For example, naturally occurring rare diamonds with positive trigons shown on
495 Fig. 1c,d best resemble figure 6 from Yamaoka et al. (1980) study, which shows experimentally
496 oxidized diamond at 4 GPa at the extreme oxidation conditions corresponding to Mn₂O₃ – MnO₂
497 oxygen fugacity buffer. We propose that there are at least two different natural mechanisms that
498 produce positive trigons on diamonds by enhancing removal rate of triply-bonded carbon atoms
499 (Angus and Dyble 1975). First, the extreme oxidation (and / or heating) experienced by
500 diamonds in the mantle source, can explain presence of extremely rare individual diamond
501 crystals found in parcels where other diamonds show no positive trigons. Second, near-surface
502 resorption event can overprint all diamonds with tiny positive trigons similar to the ones
503 described here on Snap Lake diamonds. As SEM imaging becomes a routine step in
504 characterization of diamond parcels, the proposed here association of positive trigons with
505 diamonds from kimberlite sheets can be further tested.

506

507

Implications

508 It has been shown that the common resorption features of diamonds such as negative trigons,
509 hexagons, and circular pits show strong association with the CO₂/CO₂+H₂O ratio and
510 temperature of the oxidizing fluid and hence may serve as a proxy of fluid in kimberlite systems
511 (e.g. Fedortchouk et al. 2007; Zhang et al. 2015). By expanding this method to positive trigons in
512 this study, we confirmed that the trigon diameter correlates with T and duration of the resorption
513 event and may be used to examine the thermal history of fluids during crystallization of a
514 kimberlite body. We also confirmed that the correlation of the diameter and the depth established

515 for negative p/b trigons exists for positive p/b trigons, and likely results from the CO₂/CO₂+H₂O
516 ratio in the fluid.

517 Our findings place some constraints on the crystallization conditions of different kimberlite
518 bodies. In the Snap Lake dyke we identified two diamond resorption events produced by the
519 kimberlite magma. The early high-P resorption occurred in all kimberlite litho-facies during the
520 ascent and produced negative trigons. The later low-P resorption event produced the positive
521 trigons on all studied Snap Lake diamonds at near-surface conditions (pressures approaching 0.1
522 MPa) by high-temperature magmatic fluid (~800 – 1100°C). Since experiments at 0.1 MPa show
523 development of positive trigons as fast as within one hour (Fedortchouk, unpublished data),
524 absence of positive trigons on diamonds from the majority of kimberlite bodies suggests very
525 quick magma cooling below ~800°C precluding the development of any late resorption features.
526 The presence of positive trigons on diamonds indicates unusual emplacement conditions. Further
527 studies are needed to clarify if such resorption events are a feature of kimberlite sheets, which do
528 not breach the surface and better preserve magmatic volatiles.

529 Solubility of H₂O and CO₂ in kimberlite-like magma (Moussallam et al, 2016) suggests
530 exsolution of both volatiles only very close to the surface within the last 2-5 km of the ascent.
531 This could drive the explosive eruption and magma fragmentation, but would not explain the
532 extremely fast ascent of kimberlites (e.g. Canil and Fedortchouk 1999, Kelley and Wartho 2000,
533 Sparks et al., 2006). A reaction between silicate xenoliths and carbonate-rich kimberlite magma
534 may exsolve CO₂ starting as deep as 70-80 km (~2.5 GPa) (Russell et al. 2012, Stone and Luth
535 2016) to drive the fast kimberlite ascent. However, the features of negative trigons on diamonds
536 indicate notable variation in CO₂/CO₂+H₂O ratio of the fluid (Fedortchouk 2015), which in some
537 kimberlites is less than 50 mol% CO₂ (Zhang, 2016). This study observed a change from the f/b

538 shape of the negative trigons (typical for H₂O-rich fluids) to p/b shape of the positive trigons
539 (typical for CO₂ –rich fluids), which may suggest CO₂ increase in the fluid during the ascent
540 through the last kilometers. Indeed, experimentally determined solubilities of H₂O and CO₂ show
541 an increase in CO₂ exsolution closer to the surface (Moussallam et al, 2016). Yet, it is not clear if
542 H₂O component in kimberlitic fluid introduced due to decompressional degassing at 2-5 km
543 below the surface could be responsible for all the observed resorption on kimberlitic diamonds.
544 Our study shows that a better understanding of P, T, and *fO*₂ of the reversal in trigon orientation
545 may provide a tool to establish the depth of exsolution and changes in the composition of
546 kimberlitic fluid. Since the development of the positive trigons is limited by P and T, this would
547 probably provide the most robust record of crystallization conditions and emplacement
548 mechanism of kimberlite magma.

549 Further testing of the proposed association of positive trigons on diamonds with kimberlite
550 sheets, can have important implications for diamond exploration. It is important to distinguish
551 between kimberlite sheets and hypabyssal kimberlites of the root zone of kimberlite pipes at the
552 early stage of a drilling program. This impact the assessment of the ore reserve calculation and
553 modelling of kimberlite body. Perhaps examining for the presence of positive trigons on micro-
554 diamonds under SEM can help better planning of drilling expenses.

555

556 **Acknowledgments**

557 We thank De Beers Canada Inc. for providing diamond samples, financial and logistical support
558 of this study, and the permission to publish the results. We thank Thomas Stachel for the help
559 with FTIR analyzes at University of Alberta, James Brenan and Eric Keltie for the help with gas-
560 mixing experiments, and Patricia Scallion for assistance with FE-SEM work at Dalhousie

561 University. Z.L. gratefully acknowledges the graduate scholarship from Cargill Food
562 Technology (Pinghu, China) Co., Ltd, and student research support from Shell. Y.F.
563 acknowledges funding from Natural Sciences and Engineering Research Council of Canada
564 (NSERC) Discovery, Engage and Collaborative Research and Development grants. AFM was
565 funded by Canada Foundation for Innovation grant to Y.F.

566

567 **References cited**

- 568 Afanasyev, A.A., Melnik, O., Porritt, L., Schumacher, J.C., and Sparks, R.S. (2014)
569 Hydrothermal alteration of kimberlite by convective flows of external water.
570 Contributions to Mineralogy and Petrology, 168: 1038. DOI 10.1007/s00410-014-1038-y
- 571 Agashev, A.M., Pokhilenko, N.P., MacDonald, J.A., Takazawa, E., Vavilov, M.A., Sobolev,
572 N.V., and Watanabe, T. (2001) A unique kimberlite–carbonatite primary association in
573 the Snap Lake dyke system, Slave Craton: evidence from geochemical and isotopic
574 studies. Slave–Kaapvaal Workshop Geological Survey of Canada, Merrickville, Ontario,
575 Canada.
- 576 Angus, J.C. and Dyble, T.J. (1975) Etching models for a {111} diamond surface: calculation of
577 trigon slopes. Surface Science, 50, 157–177.
- 578 Arima, M. and Kozai, Y. (2008) Diamond dissolution rates in kimberlitic melts at 1300–1500
579 degrees C in the graphite stability field. European Journal of Mineralogy, 20, 357–364.
- 580 Boyd, S.R., Kiflawi, I., and Woods, G.S. (1994) The relationship between infrared absorption
581 and the A defect concentration in diamond. Philosophical Magazine B 69, 1149–1153.
- 582 Boyd, S.R., Kiflawi, I., and Woods, G.S. (1995) Infrared absorption by the B nitrogen aggregate
583 in diamond. Philosophical Magazine B 72, 351–361.

- 584 Canil, D. and Fedortchouk, Y. (1999) Garnet dissolution and the emplacement of kimberlites.
- 585 Earth and Planetary Science Letters, 167, 227–237.
- 586 Evans, T. and Sauter, D.H. (1961) Etching of diamond surfaces with gases. Philosophical
587 Magazine, 6, 429–440.
- 588 Evans, T and Phaal, C. (1962) The kinetics of the diamond-oxygen reaction. In: Proceedings of
589 the Fifth conference on Carbon, 147–153. Pergamon Press, Oxford.
- 590 Fedortchouk, Y., and Canil, D. (2004) Intensive variables in kimberlite magmas, Lac de Gras,
591 Canada and implications for diamond survival. Journal of Petrol 45, 1725–1745.
- 592 Fedortchouk, Y., Canil, D., and Semenets, E. (2007) Mechanisms of diamond oxidation and their
593 bearing on the fluid composition in kimberlite magmas. American Mineralogist, 92,
594 1200–1212.
- 595 Fedortchouk, Y. and Canil, D. (2009) Diamond oxidation at atmospheric pressure: development
596 of surface features and the effect of oxygen fugacity. European Journal of Mineralogy, 21,
597 623–635.
- 598 Fedortchouk, Y., Matveev, S., Carlson, J.A. (2010): H₂O and CO₂ in kimberlitic fluid as
599 recorded by diamonds and olivines in several Ekati Diamond Mine kimberlites,
600 Northwest Territories, Canada. Earth and Planetary Science Letters, 289, 549–559.
- 601 Fedortchouk Y. (2015) Diamond resorption features as a new method for examining conditions
602 of kimberlite emplacement. Contributions to Mineralogy and Petrology, 170:36 doi
603 10.1007/s00410-015-1190-z
- 604 Fedortchouk, Y., Chinn, I.L., and Kopylova, M.G. (2017) Three styles of diamond resorption in
605 a single kimberlite: Effects of volcanic degassing and assimilation. Geology, 45, 871–874.
606 doi:10.1130/G39066.1

- 607 Field, M., Gernon, T.M., Mock, A., Walters, A., Sparks, R.S.J., and Jerram, D.A. (2009)
608 Variations of olivine abundance and grain size in the Snap Lake kimberlite intrusion,
609 Northwest Territories, Canada: A possible proxy for diamonds. *Lithos*, 112, 23-25.
- 610 Fulop, A., Kopylova M.G., Ellemers, P., and Squibb, C. (2017) Geology of the Snap Lake
611 kimberlite dyke, Northwest Territories, Canada, and its metasomatic interaction with
612 granite. 11th International Kimberlite Conference Extended Abstract No. 11IKC-4528.
- 613 Gernon, T.M., Field, M., and Sparks, R.S.J. (2012) Geology of the Snap Lake kimberlite
614 intrusion, Northwest Territories, Canada: field observations and their interpretation.
615 *Journal of the Geological Society, London*, 169, 1-16.
- 616 Harris, J.W. and Vance, E.R. (1974) Studies of the reaction between diamond and heated
617 kimberlite. *Contributions to Mineralogy and Petrology*, 47, 237-244.
- 618 Heaman, L.M., Kjarsgaard, B.A., and Creaser, R.A. (2003) The timing of kimberlite magmatism
619 in North America: implications for global kimberlite genesis and diamond exploration.
620 *Lithos*, 71, 153–184.
- 621 Heaman, L.M., Kjarsgaard, B.A., and Creaser, R.A. (2004) The temporal evolution of North
622 American kimberlites. *Lithos*, 76, 377-397.
- 623 Kelley, S.P. and Wartho, J.-A. (2000) Rapid kimberlite ascent and the significance of Ar-Ar ages
624 in xenolith phlogopites. *Science*, 289, 609-611.
- 625 Khokhryakov, A.F. and Pal'yanov, Y.N. (2010) Influence of the fluid composition on diamond
626 dissolution forms in carbonate melts. *American Mineralogist*, 95, 1508–1514.
- 627 Kopylova, M.G., Mogg, T., and Smith, B.H.S. 2010. Mineralogy of the snap lake kimberlite,
628 Northwest Territories, Canada, and compositions of phlogopite as records of its
629 crystallization. *The Canadian Mineralogist*, 48, 549-570.

- 630 Li Z. (2017) Micro-morphology and Resorption features of Diamonds from Snap Lake and Ekati
631 Kimberlites (Canada) as an Indicator of Kimberlite Emplacement Conditions. 197 p.
632 M.Sc. thesis, Dalhousie University, Halifax.
- 633 Luttge A. (2006) Crystal dissolution kinetics and Gibbs free energy. Journal of Electron
634 Spectroscopy and Related Phenomena, 150, 248–259.
- 635 McCollom, T.M., and Seewald, J.S. (2013) Serpentinites, Hydrogen, and Life. Elements 9, 129–
636 134.
- 637 Mitchell, R.H. (2013) Paragenesis and oxygen isotopic studies of serpentine in kimberlite, in
638 Pearson, D.G., et al., eds., Proceedings of 10th International Kimberlite Conference,
639 Volume 1: Special Issue of the Journal of the Geological Society of India: New Delhi,
640 Springer, p. 1–12, doi: 10.1007/978-81-322-1170-9_1.
- 641 Mogg, T., Kopylova, M.G., Scott Smith, B.H., and Kirkley, M. (2003) Petrology of the Snap
642 Lake kimberlite. In 8th International Kimberlite Conference Long Abstract.
- 643 Moussallam, Y., Morizet, Y., and Gaillard, F. (2016) H₂O–CO₂ solubility in low SiO₂-melts
644 and the unique mode of kimberlite degassing and emplacement. Earth and Planetary
645 Science Letters, 447, 151–160, doi: 10.1016/j.epsl.2016.04.037.
- 646 Ogilvie-Harris, R.C., Sparks, R.S.J., Field, M., and Gernon, T.M. (2009) The Geochemistry of
647 the Snap Lake kimberlite dyke, NW Territories, Canada: Phlogopite and Spinel. EOS,
648 Transactions, American Geophysical Union, 90, Abstract V33D-01.
- 649 Phaal, C. (1965) Surface studies of diamond. Industrial Diamond Review, 25, 486–489 and 591–
650 595.
- 651 Robinson, D.N. (1979) Surface Textures and Other Features of Diamonds. 221 p., Ph.D. thesis.
652 The University of Cape Town, Cape Town.

- 653 Russell, J.K., Porritt, L.A., Lavallée, Y., and Dingwell, D.B. (2012) Kimberlite ascent by
654 assimilation fuelled buoyancy. *Nature*, 481, 352–356, doi: 10.1038/nature10740.
- 655 Scott Smith, B.H., Nowicki, T.E., Russell, J.K., Webb, K.J., Mitchell, R.H., Hetman, C.M.,
656 Harder, M., Skinner, E.M.W., and Robey, J.A. (2013) Kimberlite terminology and
657 classification, in Pearson, D.G., et al., eds., *Proceedings of 10th International Kimberlite*
658 *Conference, Volume 2: Special Issue of the Journal of the Geological Society of India:*
659 New Delhi, Springer, p. 1–18, doi: 10.1007/978-81-322-1173-0_1.
- 660 Sparks, R.S.J., Baker, L., Brown, R.J., Field, M., Schumacher, J., Stripp, G., Walters, A. (2006)
661 Dynamical constraints on kimberlite volcanism. *Journal of Volcanology and Geothermal*
662 *Research*, 155, 18–48.
- 663 Stachel, T., Banas, A., Muehlenbachs, K., Kurszlaukis, S., Walker, E. (2006) Archean diamonds
664 from Wawa (Canada): samples from deep cratonic roots predating cratonization of the
665 Superior Province. *Contributions to Mineralogy and Petrology*, 151, 737–750.
- 666 Stone, R.S., and Luth, R.W. (2016) Orthopyroxene survival in deep carbonatite melts:
667 Implications for kimberlites. *Contributions to Mineralogy and Petrology*, 171, 63, doi:
668 10.1007/s00410-016-1276-2.
- 669 Stripp, G.R., Field, M., Schumacher, J., Sparks, R.S.J., and Cressey, G. (2006) Post-
670 emplacement serpentinization and related hydrothermal metamorphism in a kimberlite
671 from Venetia, South Africa. *Journal of Metamorphic Geology*, 24, 515–534, doi:
672 10.1111/j.1525-1314.2006.00652.x.
- 673 Stuble, M.P. (2000) Geology of the Northern Snap Lake area. De Beers Canada Mining,
674 internal report prepared for Winspear Resources, with accompanying 1:10,000 scale map.

- 675 Yamaoka, S., Kanda, H., and Setaka, N. (1980) Etching of diamond octahedrons at high
676 temperatures and pressures with controlled oxygen partial pressure. Journal of Material
677 Sciences, 15, 332–336.
- 678 Zhang, Z., Fedortchouk, Y., and Hanley J.J. (2015) Evolution of diamond resorption in a silicic
679 aqueous fluid at 1–3 GPa: Application to kimberlite emplacement and mantle
680 metasomatism. Lithos, 227, 179–193.
- 681 Zhang, Z. (2016) Diamond resorption morphology as a fluid proxy in diamond-bearing
682 environments: constraints from empirical and experimental studies. 302 p. Ph.D. thesis,
683 Dalhousie University, Halifax.
- 684

685 **Figure Captions**

686

687 Figure 1 - A) Positive and negative trigons on {111} diamond face and their formation due to
688 relative rates of propagation of step 1 (positive trigons) and step 2 (negative trigons) (after
689 Yamaoka et al. 1980). B) Truncated trigon on {111} diamond face with lengths of positive (L_{pos})
690 and negative (L_{neg}) micro-faces shown (after Zhang 2016). C) Natural diamond of unknown
691 geographic origin with abundant positively oriented trigons and imbricate wedges. D) Natural
692 diamond (octahedral macle twin) with positively oriented trigons, fine transverse hillocks on
693 resorbed dodecahedral surfaces and imbricate wedge markings.

694

695 Figure 2 – Geology of the Snap Lake kimberlite dyke. A) The location and shape of the dyke. B)
696 Distribution of the six kimberlite litho-facies within Snap Lake dyke relative to the contact with
697 the two types of the country-rocks (after Fulop et al. 2017).

698

699 Figure 3 – Classification approach for trigonal etch pits on diamond based on the bottom and
700 wall geometries (modified from Zhang et al. 2015). The pits are defined as having V type walls
701 when $[\alpha_1 - \alpha_2] < 1^\circ$ and as f/b when $[\beta_1 - \beta_2] < 1^\circ$.

702

703 Figure 4 – Microphotographs of sixteen Snap Lake diamonds, on which positive and negative
704 trigons were studied by AFM.

705

706 Figure 5 - Development of positively-oriented micro-faces on negative trigons on Snap Lake
707 diamonds (A – F) and in experiments at 1250°C and 1 GPa with CO₂-rich fluids (modified from
708 Zhang 2016) (G – I). A – C – development of truncated corners of trigons on Snap Lake
709 diamonds; D – F – trigon-hexagons and hexagons on Snap Lake diamonds; G – I – negative
710 trigons from the Zhang (2016) experiments showing curvature of trigon edges accompanying
711 truncation of the corners with positive micro-faces. The degree of corner truncation
712 ($L_{\text{pos}}/L_{\text{pos}}+L_{\text{neg}}$ ratio) increases from (G) to (I). All images are AFM scans.

713

714 Figure 6 – Distribution of positive trigons on Snap Lake diamonds: on resorbed THH faces (a,b),
715 on {111} faces (c, d, e, f), and inside the negative trigons (g, h). The boxes on the left images
716 show the location of the close-up area displayed on the right. a, b, c, e, g – microphotographs; d,
717 f, h – AFM images.

718

719 Figure 7 – Diameter vs. depth of positive trigons on Snap Lake diamonds from different
720 kimberlite litho-facies based on the AFM measurements. For the trigons types see Fig. 9.

721

722 Figure 8 – Diameter of positive trigons on diamonds from different litho-facies of Snap Lake
723 kimberlite. A) The choice of a representative maximum trigon size of the positive trigons on
724 individual diamonds studied with optical microscope or SEM. B) Use of the above approach to
725 establish the proportions of diamonds with a maximum size of the positive trigons $\leq 3 \mu\text{m}$,
726 between 3-5 μm , and $\geq 5 \mu\text{m}$ in each kimberlite facies. C) The diameter range of the individual
727 positive trigons measured with AFM on Snap Lake diamonds from different kimberlite facies.

728

729 Figure 9 – Morphological types of positive trigons on Snap Lake diamonds based on the AFM
730 profiles.

731

732 Figure 10 – Etching of diamond surface in experiments with Na_2CO_3 - NaCl melt conducted at 0.1
733 MPa, 700°C and 800°C and $f\text{O}_2$ corresponding to that of the air and pure CO_2 gas. AFM images
734 of diamond surface before and after the runs at 700°C show development of positive trigons in
735 air and no sign of resorption in CO_2 .

736

737 Figure 11 - A) The relationship between the ratio $L_{\text{pos}}/L_{\text{pos}}+L_{\text{neg}}$ and the diameter of trigonal etch
738 pits on diamonds from different kimberlite facies showing that the trend defined by diamonds
739 from the fresh HK1-HK2 kimberlites is different from the trend defined by diamonds from more
740 altered kimberlites (HK4, 5, 6). B) L_{pos} values of etch pits measured on individual diamonds
741 from different kimberlite facies (the diamond labels are shown along the x-axes, the number of
742 measured pits is shown in brackets).

743

744 Figure 12 - Atom removal process and development of trigonal etch pits on {111} diamond
745 surfaces (from Angus and Dyble 1975) showing development of a negative trigon (B) from an
746 arbitrary hole in the outer layer (A) after sequential removal of doubly-bonded atoms. X is a top
747 layer atom bonded to the layer below. 0 is a top layer atom not bonded to the layer below.

748

749

750 **Tables**

751 Table 1 – Summary of the sources of uncertainty in AFM measurements.

752 Table 2 –AFM details and nitrogen data for the fourteen diamond from Snap Lake kimberlite
753 studied by AFM.

754

755 **Electronic supplementary materials**

756 ES table 1 – AFM data of Snap Lake diamonds

757

758

759

760

761

Table 1 Summary of the sources of uncertainty in AFM measurements.

Parameter	Source of uncertainty		Total uncertainty
	Systematic Errors	Random Errors	
Diameter	AFM uncertainty after calibration (1.4%); Tilt of the raw image before Plane Fit operation (<0.2%)	Subjective selection of measurements (0.6%)	<2.5%
Depth	AFM uncertainty after calibration (1.4%); the remaining tilt and the compression of the image after the Plane Fit operation (<4%);	Subjective selection of measurements (0.3%)	<6%
$\alpha_{\{111\}}$	AFM uncertainty after calibration (<2°); Tilt of the raw image and the remaining tilt after the Plane Fit operation (<1°)	Subjective selection of measurements (<1°)	<4°

Table 2 AFM details and nitrogen data (from FTIR) for the fourteen diamond from Snap Lake kimberlite studied on AFM.

Diamond	Lithology	# sides scanned	# of etch pits scanned			Nitrogen defects	
			positive trigons	negative trigons	hexagons	N total ppm	%B defects
SNP2-1	HK1	1	11	3	1	526.9	20.3
SNP8-9		1	11	0	0	1027.3	16.5
SNPO13-2		1	9	2	1	893.2	36.0
SNP3-6	HK2	1	8	0	1	46.6	97.9
SNP3-8		1	10	2	0	1431.9	4.8
SNP6-1		1	19	8	0	321.6	1.1
SNP9-1		2	11	0	1	344.2	54.2
SNPO9-1		1	8	0	0	388.3	58.2
SNP1-9	HK4	1	10	0	0	1021.9	50.4
SNP10-9		1	9	1	2	502.5	26.7
SNP5-3	HK5	1	12	11	2	100.4	57.6
SNPO12-2	HK6	1	9	4	0	178.5	37.5
SNPO12-3		2	18	2	0	246.6	43.1
SNPO12-8		1	9	1	0	17	65.9

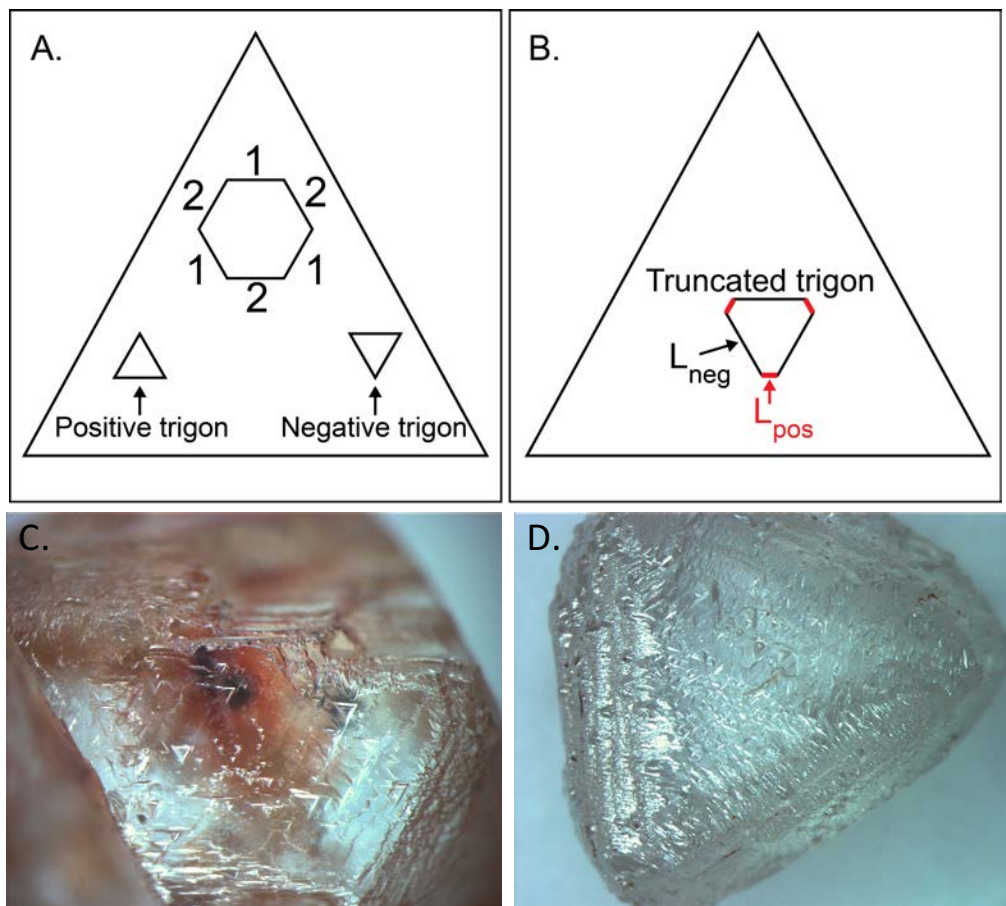


Figure 1

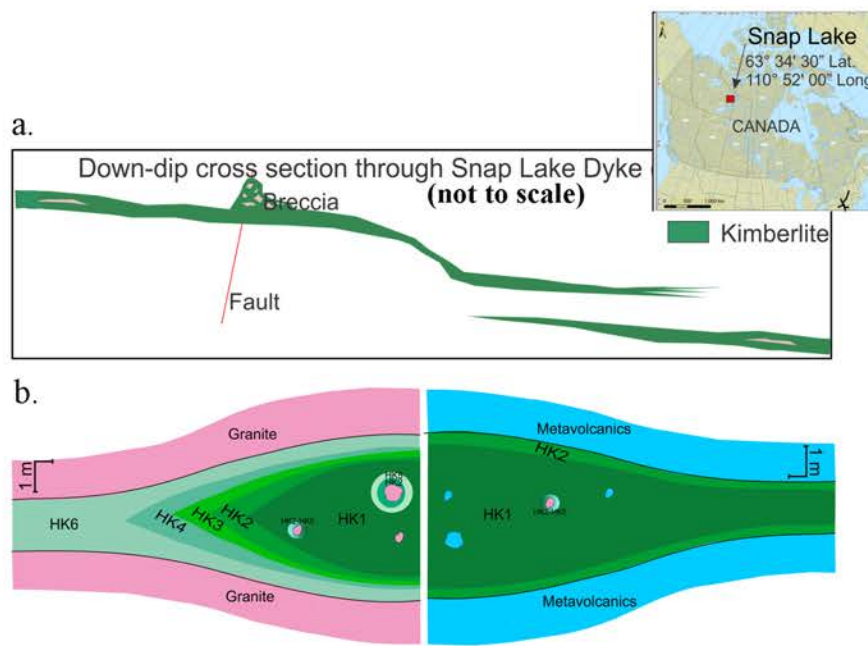


Figure 2

Bottom type Wall type	Flat-bottomed (f/b)	Point-bottomed (p/b)	Curved bottom (c/b)
V type			Not observed
U type			
		Bottom type is determined by $\beta_1 + \beta_2$	
Y type			Not observed

Figure 3

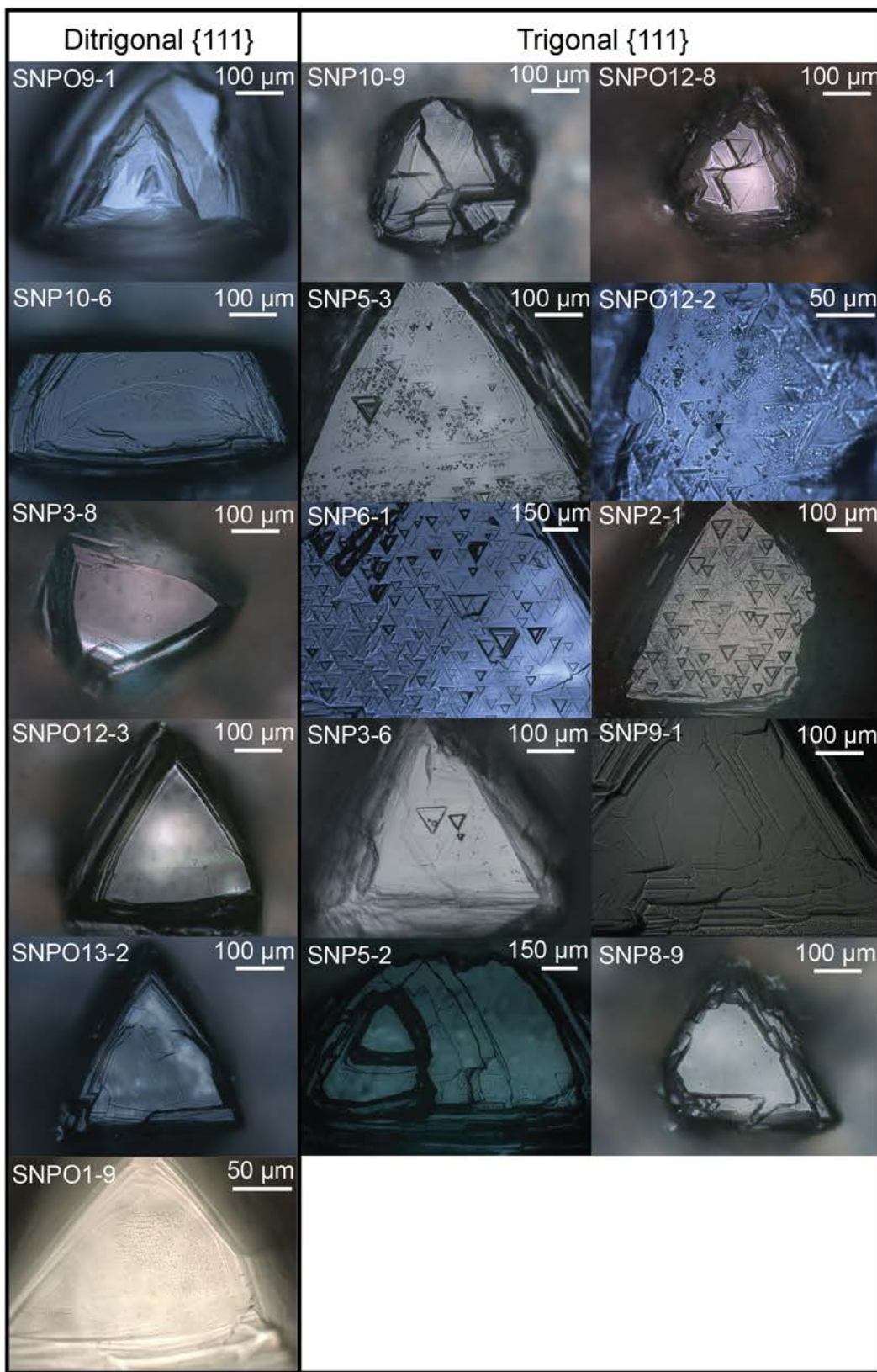
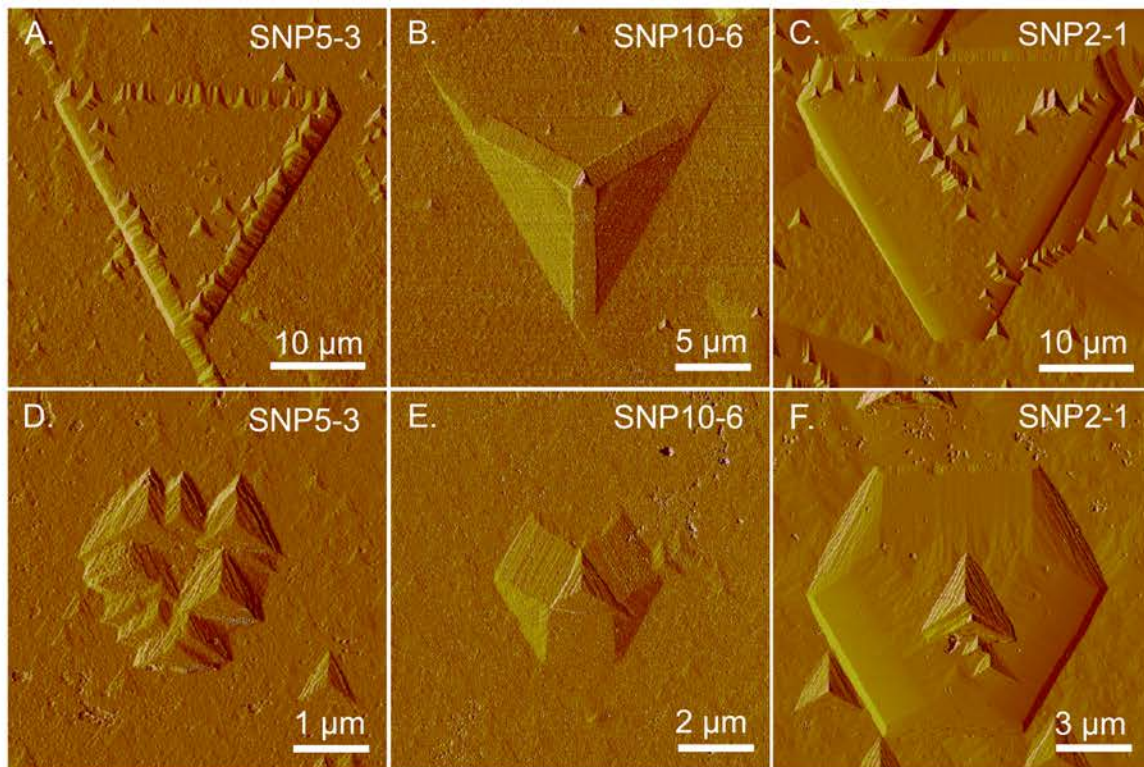


Figure 4

Snap Lake diamonds (this study)



Experiments in C-O-H fluids (after Zhang, 2016)

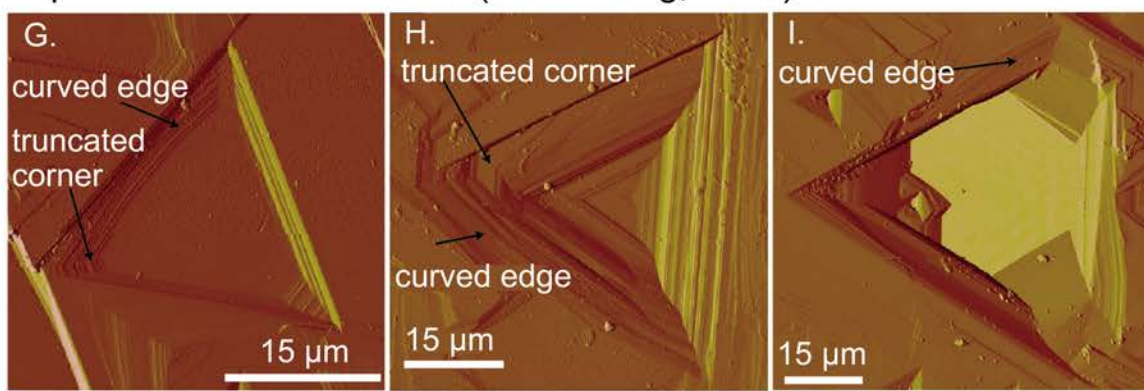


Figure 5

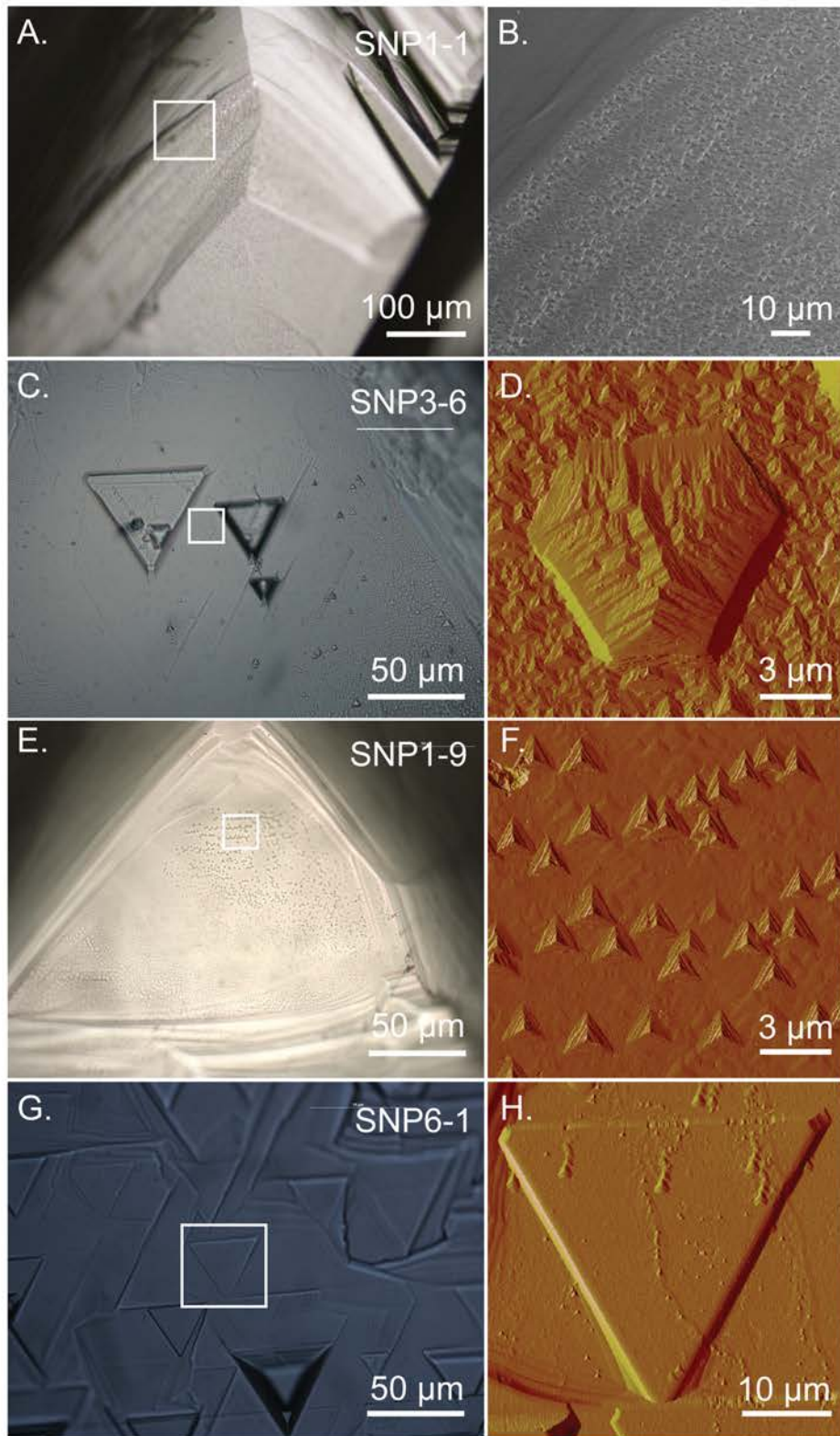


Figure 6

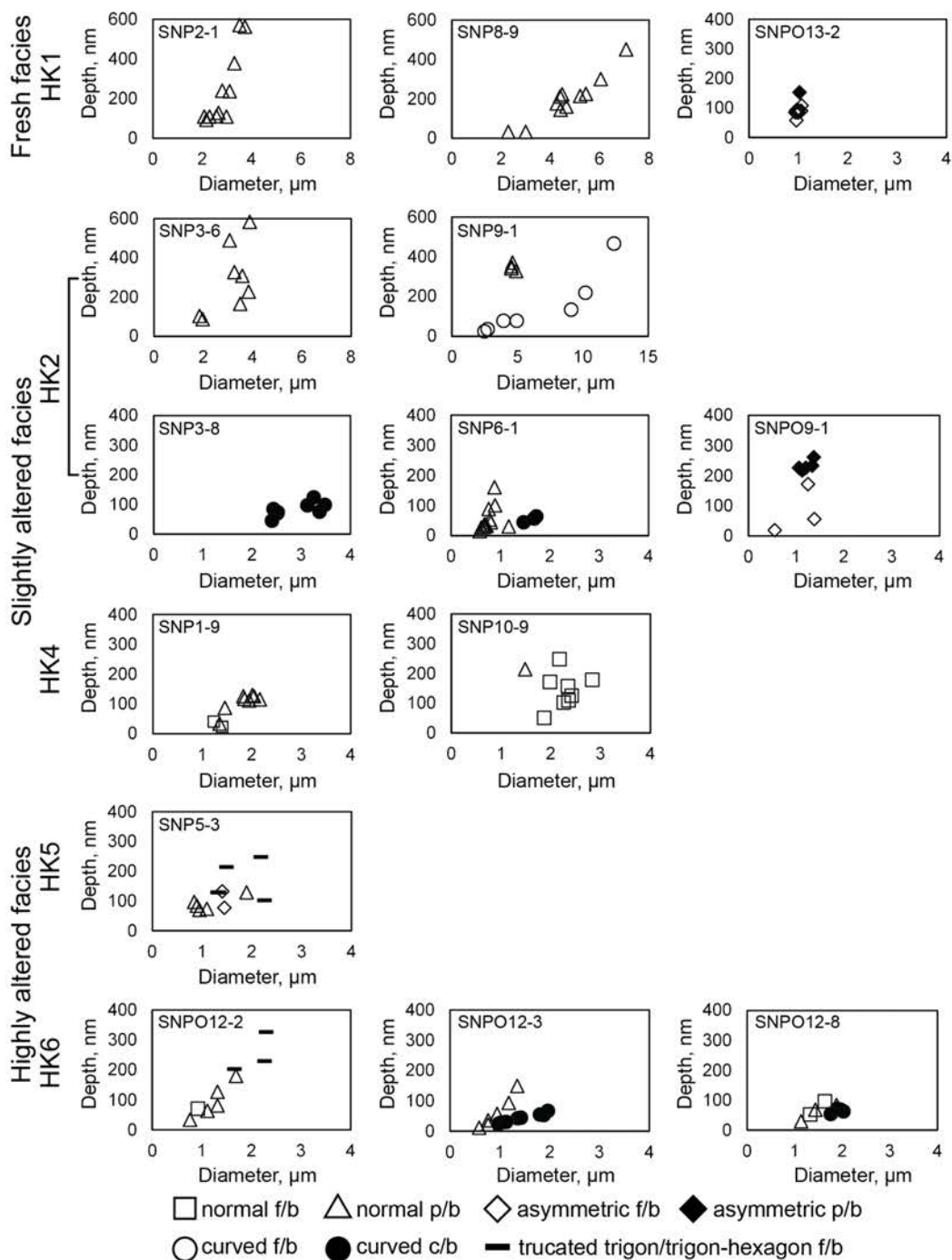


Figure 7

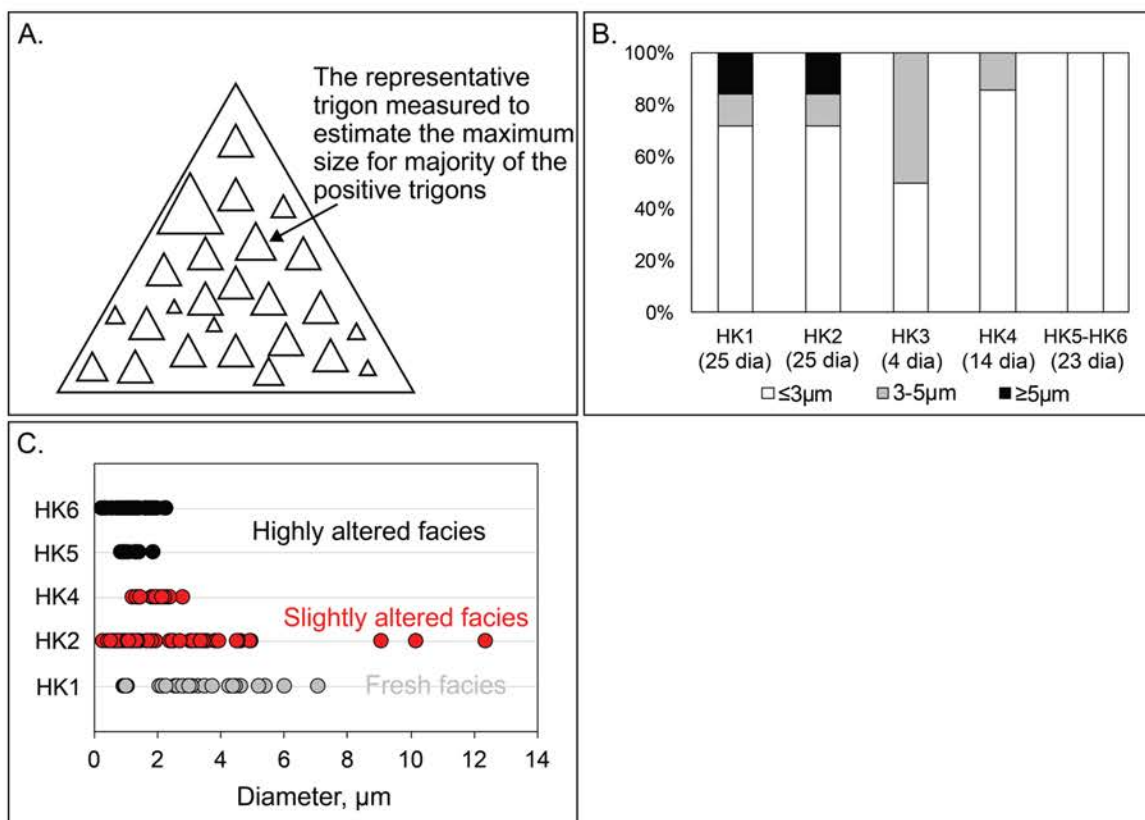


Figure 8

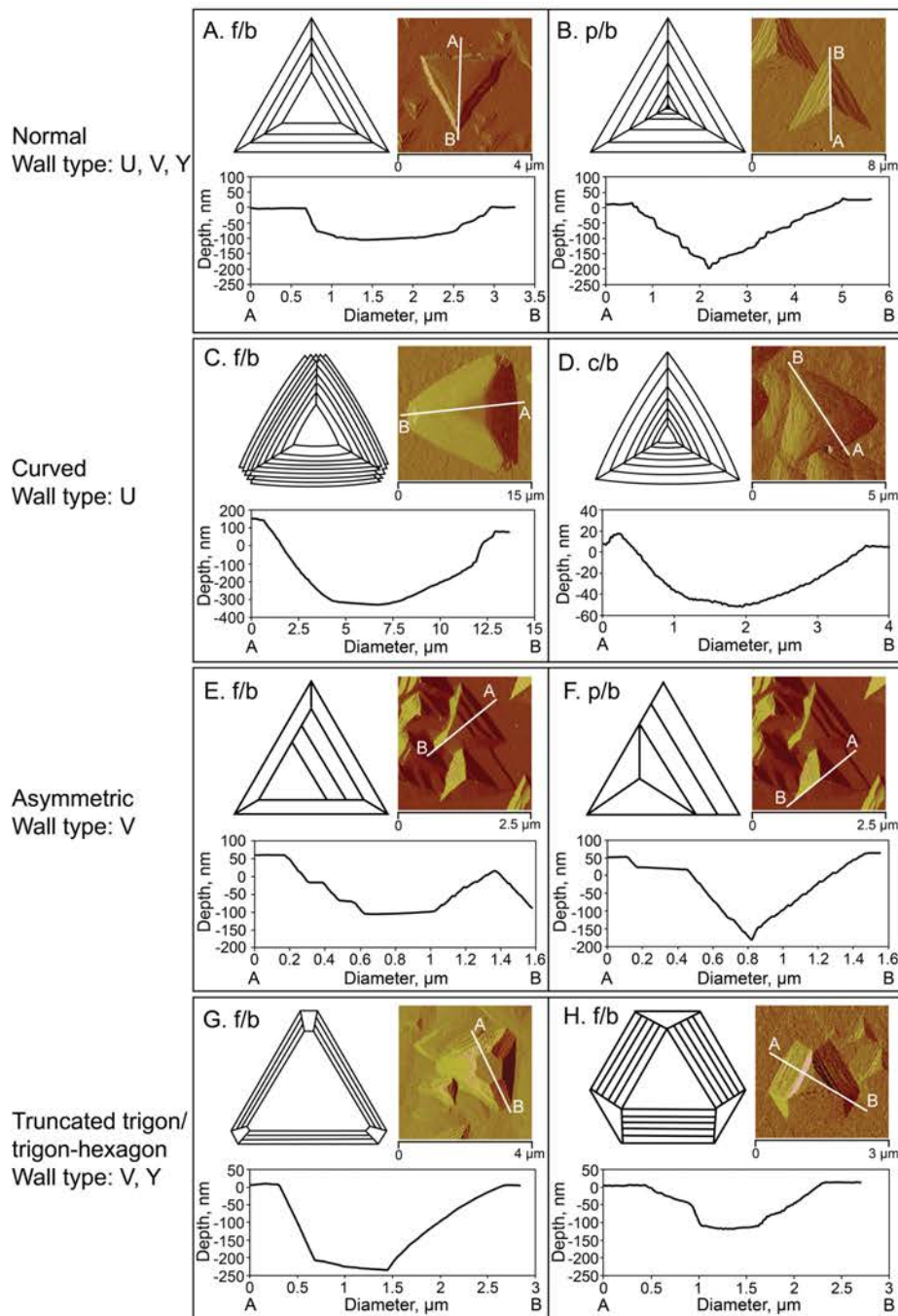


Figure 9

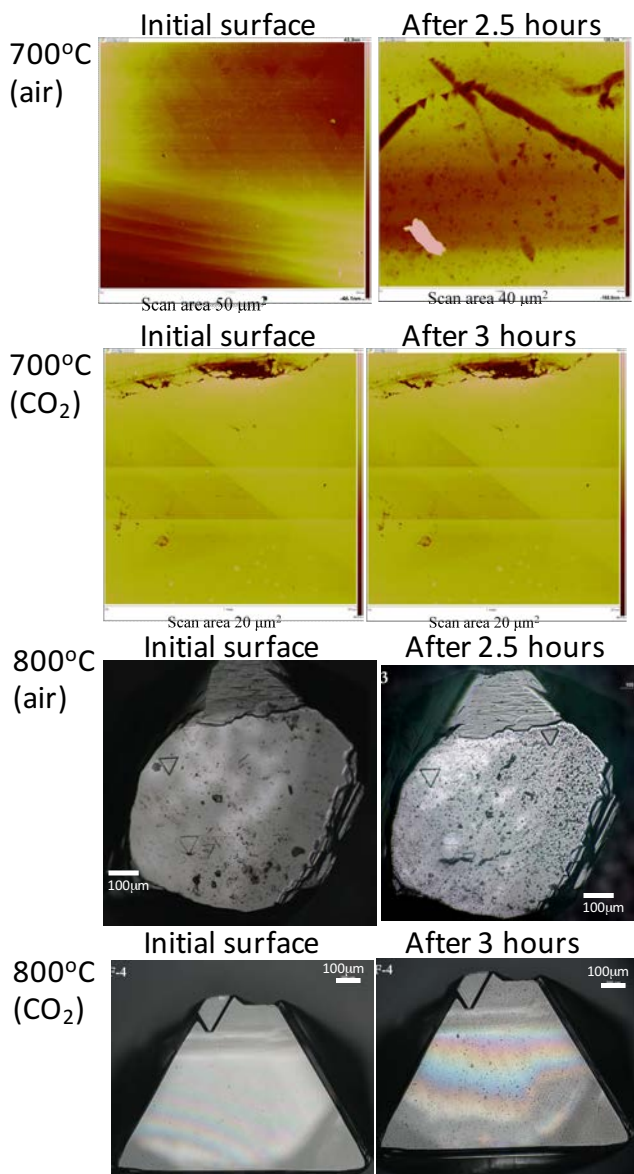


Figure 10

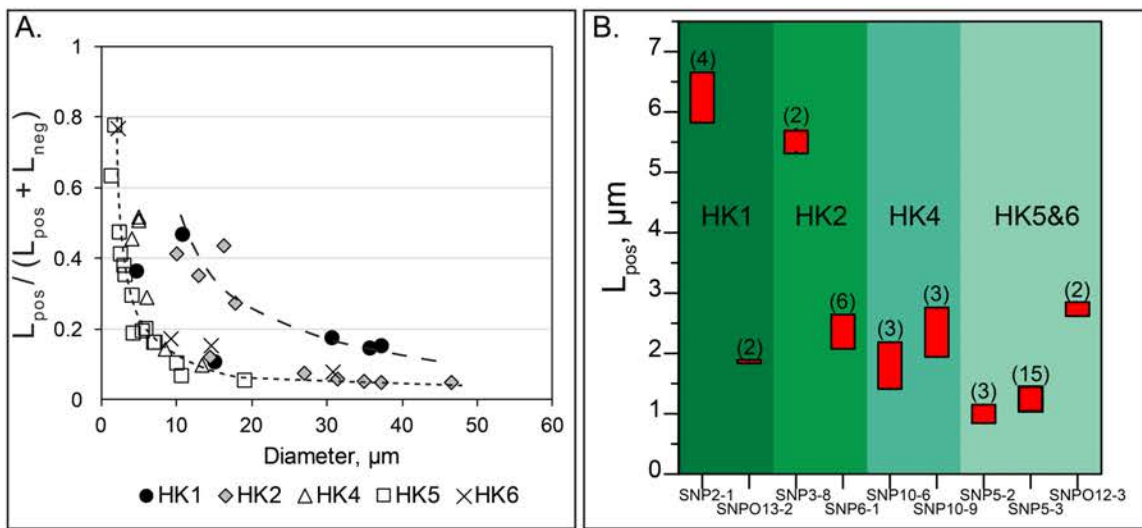


Figure 11

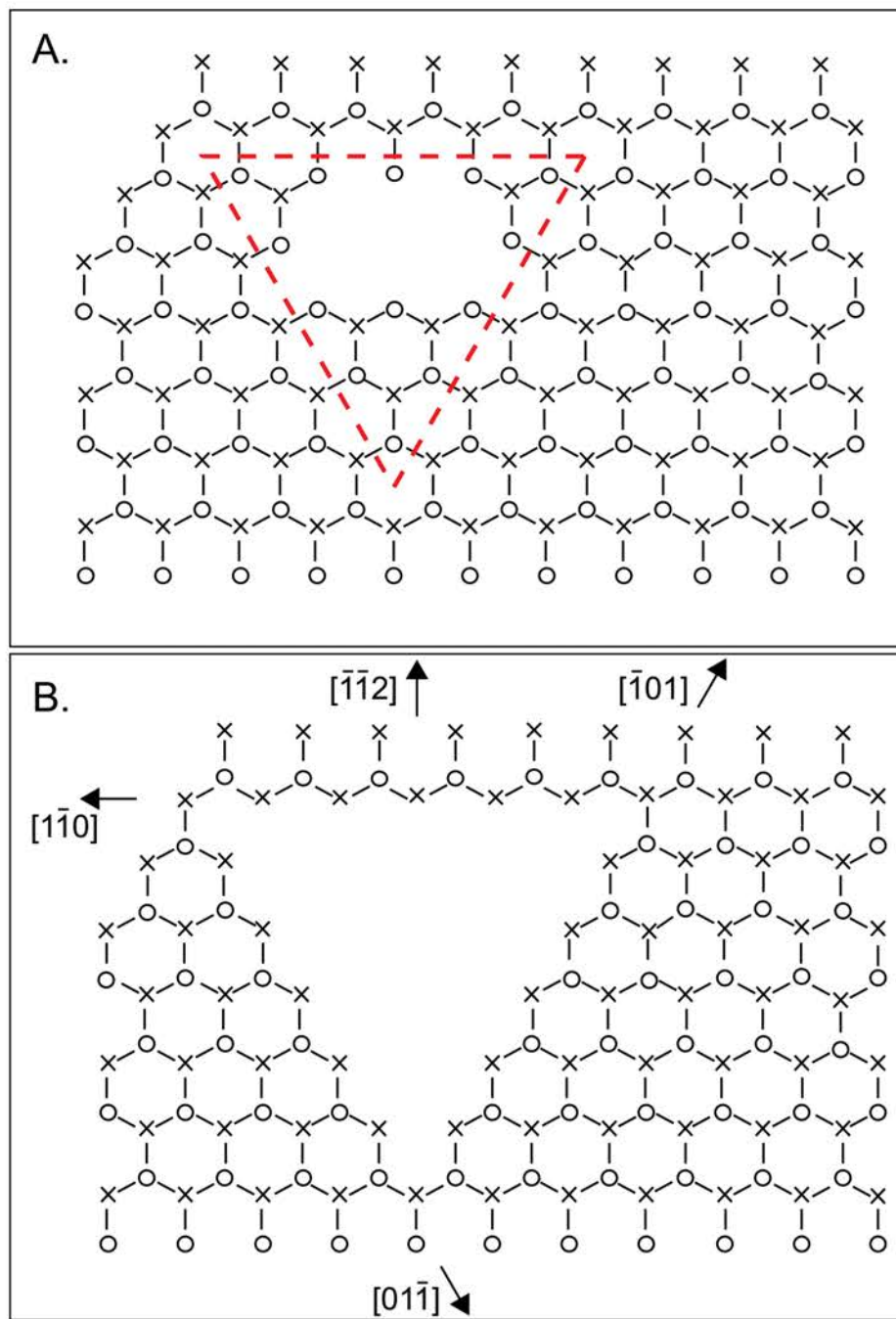


Figure 12